



# Effect of different hole transport materials on photovoltaic properties in solar cells based on $\text{MAPbI}_3$ perovskite

MASOUD MEHRABIAN and ELHAM NOROUZI AFSHAR\*

Department of Physics, Faculty of Basic Science, University of Maragheh, PO Box, 55181-83111 Maragheh, Iran

\*Author for correspondence (e.afshar@tabrizu.ac.ir; noroozi.afshar@yahoo.com)

MS received 27 May 2021; accepted 26 June 2021

**Abstract.** Three photovoltaic devices based on  $\text{CH}_3\text{NH}_3\text{PbI}_3$  ( $\text{MAPbI}_3$ ) perovskite using molybdenum oxide ( $\text{MoO}_3$ ), spiro-OMeTAD and poly(3-hexylthiophene-2,5-diyl) (P3HT) as hole transport materials (HTMs) with different highest occupied molecular orbital (HOMO) energy levels were simulated under AM 1.5G illumination of  $1000 \text{ W m}^{-2}$  intensity and light to electricity power conversion efficiency (PCE or  $\eta$ ) of 16.12, 14.67 and 6.6% were obtained, respectively. The main aim of this study is to find an optimal HTM for perovskite solar cells (PSC). The device with  $\text{MoO}_3$  delivered the maximum fill factor of 76.49% and short-circuit current ( $J_{\text{SC}}$ ) of  $21.38 \text{ mA cm}^{-2}$ , but suffered from the lower open-circuit voltage ( $V_{\text{OC}}$ ) compared to a device containing spiro-OMeTAD and P3HT. However, charge recombination and losses at interfaces between layers are two main factors that restrict cell performance. In this study, it is shown that  $\text{MoO}_3$  not only passivates the interfacial traps, but also enhances the charge extraction of the device. The enhancement in the performance of PSC by  $\text{MoO}_3$  passivation compared to two other devices is discussed in detail.

**Keywords.** Perovskite solar cell;  $\text{MAPbI}_3$ ; spiro-OMeTAD; P3HT;  $\text{MoO}_3$ .

## 1. Introduction

Organic photovoltaics (OPVs) have attracted attention due to the advantages of low-cost, easy processing and environmental friendliness.

Recently, the performance of OPVs based on bulk heterojunction (BHJ) structure has significantly improved. In the concept of BHJ devices, the active layer is composed of a blend of electron donor and electron acceptor materials. In general, photovoltaic devices with inverted structures are more stable than those with direct structures [1].

It was reported that there are some important purposes by using the hole transport layer (HTL) in perovskite solar cells (PSC). Using HTL, avoids direct contact of the metal electrode with the electron transport layer (ETL) to increase the conductivity of contact, which leads to a decrease in the recombination of electrons and holes. Using HTL, also increases the internal quantum efficiency (IQE) of a device by reducing the losses of charges at the interfaces. Finally, using this layer, increases the reflectivity of the back electrode, leading to a second path of the light through the absorber [2].

In 2012, Zhong *et al* [3] reported a solar cell with FTO/TiO<sub>2</sub>/Cds/N719/P3HT/Au and maximum power conversion efficiency (PCE) of 1.06% with  $V_{\text{OC}} = 0.51 \text{ V}$ ,  $J_{\text{SC}} = 5.34 \text{ mA cm}^{-2}$  and FF = 38%.

In 2020, Nithya *et al* [4] simulated a solar cell containing CuI as hole transport material (HTM) with a structure of ITO/CuI/PBDB-T/ITIC/PFN-Br/Ag, and the technological parameters on the output performance of the device was investigated. The photovoltaic properties of  $V_{\text{OC}} = 0.97 \text{ V}$ ,  $J_{\text{SC}} = 20.15 \text{ mA cm}^{-2}$ , FF = 79.59% and  $\eta = 15.68\%$  were obtained.

In 2018, Chen *et al* [5] applied P3HT as HTM in solar cell with FTO/TiO<sub>2</sub>/C60/Cs<sub>2</sub>TiBr<sub>6</sub>/P3HT/Au structure and reported a PCE of 3.22% with  $V_{\text{OC}} = 1.02 \text{ V}$ ,  $J_{\text{SC}} = 5.69 \text{ mA cm}^{-2}$  and FF = 56.4%

In 2019, Wang *et al* [6] used P3HT interlayer to improve the photovoltaic properties of carbon-based CsPbBr<sub>3</sub> perovskite device with  $V_{\text{OC}} = 1.36 \text{ V}$ ,  $J_{\text{SC}} = 7.02 \text{ mA cm}^{-2}$ , FF = 68% and  $\eta = 6.49\%$ , was obtained. In 2020, Hu *et al* [7] reported a perovskite solar cell using spiro-OMeTAD HTM with FTO/TiO<sub>2</sub>/perovskite/spiro-OMeTAD/Au structure and maximum PCE of 18.4% with  $V_{\text{OC}} = 1.1 \text{ V}$ ,  $J_{\text{SC}} = 23.1 \text{ mA cm}^{-2}$  and FF = 72%, was obtained by substituting the usual chlorobenzene solvent with pentachloroethane. In 2020, Li *et al* [8] reported a device using spiro-OMeTAD as an HTM and improved the photovoltaic performance of PSCs by solvent treatment of spiro-OMeTAD film processed from non-benzene solvent. They reported the highest PCE of PSCs about 19%. In 2013, Simchi *et al* [9] used MoO<sub>3</sub> as back contact of Cu(InGa)Se<sub>2</sub> thin film solar cells and PCE of 14% with  $V_{\text{OC}} = 0.64 \text{ V}$ ,  $J_{\text{SC}} = 28.4 \text{ mA cm}^{-2}$

and FF = 78.1%, was obtained. In 2009, Hori *et al* [10] investigated the MoO<sub>3</sub> buffer layer effect on photovoltaic properties of solar cells with (ITO)/C60/poly(3-hexylthiophene) (PAT6)/Au structure. It was shown that the photovoltaic properties were improved by inserting a MoO<sub>3</sub> as a cathode buffer layer. For the device without MoO<sub>3</sub> layer, the  $V_{OC}$ ,  $J_{SC}$ , FF and  $\eta$  were 0.29 V, 4.21 mA cm<sup>-2</sup>, 39.8 and 0.49%, respectively. While these parameters improved to 0.4 V, 5.08 mA cm<sup>-2</sup>, 54.9 and 1.12%, respectively, by inserting the MoO<sub>3</sub> layer. In our previous work, the effect of thickness of the graphene oxide (GO) layer in solar cells based on CsPbBr<sub>3</sub> was investigated using SCAPS software. Results showed that a PCE of 10.91% was obtained for the GO layer with a thickness of 40 nm. In the present study, inverted planer perovskite devices with different HTMs are simulated using 1D simulator SCAPS [11].

## 2. Simulation

### 2.1 Results and discussion

All planer PSCs which are simulated in the present study, consist of transparent conducting oxide (TCO)/TiO<sub>2</sub>/MAPbI<sub>3</sub>/HTM/metal contact, as shown schematically in figure 1 (top). Indium tin oxide (**ITO**) and silver (Ag) are applied as TCO layer and metal contact, respectively. MoO<sub>3</sub>, spiro-OMeTAD and P3HT are used as HTMs. The schematic diagram of the energy levels of simulated structures is shown in figure 1 (down).

As shown in figure 1 (down), the highest occupied molecular orbital (HOMO) level of MoO<sub>3</sub>, spiro-OMeTAD and P3HT layers are located at -5.5, -5.25 and -5.2 eV, respectively [12–17]. The parameters of the materials used in this simulation are listed in table 1.

Short circuit current density–voltage ( $J$ – $V$ ) curves as well as external quantum efficiency (EQE) of solar cells with different HTMs are shown in figure 2a and b, respectively. The photovoltaic parameters of devices are summarized in table 2.

As listed in table 2, the PCE of 14.67% was obtained for the device with spiro-OMeTAD. Whereas there is not much difference in HOMO levels of P3HT and spiro-OMeTAD, for the device using the P3HT hole conductor, and the result was rather different with PCE of 6.6%.

However, the hole mobility of the spiro-OMeTAD and P3HT are about  $2 \times 10^{-4}$  and  $10^{-5}$  cm<sup>2</sup> Vs<sup>-1</sup>, respectively [18]. Higher hole mobility leads to facilitate the electron–hole separation in the interfaces. This difference in hole mobility might explain the higher performance.

In organic semiconductors, a bound electron–hole pair (exciton) is generated upon photon absorption. Excitons are generated through active layer (MAPbI<sub>3</sub>). As holes tend to move upward in transitions between layers, they are easily pumped from MAPbI<sub>3</sub> to HTM, because there is no barrier to flow photo-generated hole towards the TiO<sub>2</sub> layer. The

minimum distance between HOMO of absorber layer and HTM belongs to MoO<sub>3</sub> which leads to obtain maximum value of  $J_{SC}$  (21.38 mA cm<sup>-2</sup>). On the other hand, in the device containing of MoO<sub>3</sub>, this level distance causes an increase in interface recombination, which reduces  $V_{OC}$  [19]. Due to the low relative dielectric permittivity ( $\epsilon_r = 3$ ) of P3HT and spiro-OMeTAD ( $\epsilon_r = 3$ ) [12,20], there is a strong Coulomb attraction between the electron and hole; therefore, the dissociation of the excitons into free charges (electrons and holes) in these layers is very unlikely under ambient conditions. The maximum FF of 76.49% was obtained in device with MoO<sub>3</sub>, because of the minimum distance between HOMO level of this layer and MAPbI<sub>3</sub> absorber.

However, the  $J_{SC}$  of 21.8, 20.10 and 19.32 mA cm<sup>-2</sup> was obtained for devices due to the variations in their EQE which is shown in figure 2b. It could be observed that as  $J_{SC}$  varies, the PCE of structure using different HTMs also varies.

It was found that MoO<sub>3</sub>, P3HT and spiro-OMeTAD exhibit EQE as much as 97.36, 96.25 and 93.5%, respectively, in the visible range. Therefore, MoO<sub>3</sub> possesses the best PCE of 16.12%.

EQE in the whole visible wavelength region is almost constant. Broad spectral response is achieved up to 800 nm wavelength consistent with the 1.55 eV band gap of the MAPbI<sub>3</sub> absorber layer. The short wavelengths are absorbed near the front surface, so the photo-generated carriers are affected by the surface recombination. Below the band gap of the perovskite (1.5 eV), no light is being absorbed resulting in a zero EQE.

Figure 3 depicts the energy band diagram of the simulated devices with different HTMs.

The thickness of TiO<sub>2</sub>, MAPbI<sub>3</sub>, MoO<sub>3</sub>, spiro-OMeTAD and P3HT is 200, 200, 150, 150 and 100 nm, respectively.

In a device with P3HT, the distance between HOMO levels of MAPbI<sub>3</sub> and P3HT is more compared to other devices, which leads to an increase in recombination rate in the interfaces. A higher recombination rate decreases FF in the device. The electron–hole generation and net recombination rates,  $G$  and  $U_n$ ,  $p$  are given by electron and hole continuity equations:

$$\frac{\partial J_n}{\partial x} + G - U_n(n, p) = 0, \quad (1)$$

$$-\frac{\partial J_p}{\partial x} + G - U_n(n, p) = 0, \quad (2)$$

where  $J_n$  and  $J_p$  are the electron and hole current densities which could be given by the diffusion coefficient of electrons and holes as below:

$$J_n = qn\mu_n E + qD_n \frac{\partial n}{\partial x}, \quad (3)$$

$$J_p = qn\mu_p E - qD_p \frac{\partial p}{\partial x}, \quad (4)$$

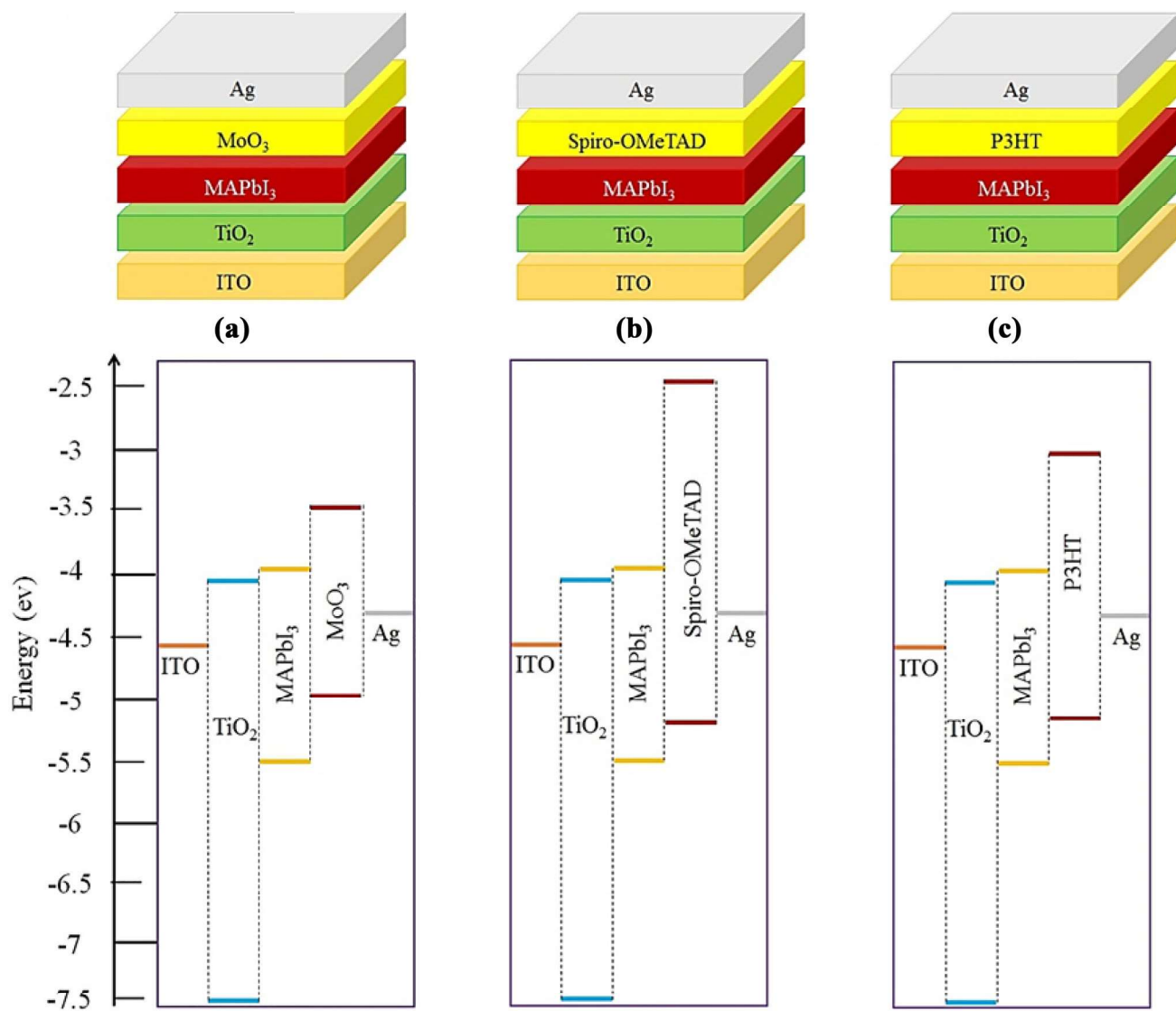


**Figure 1.** (Top) Configuration of devices with different HTMs used in the simulation. (Down) Corresponding energy levels of layers.

**Table 1.** Photovoltaic parameters of perovskite solar cells with different absorber layers.

Layer	TiO <sub>2</sub>	MAPbI <sub>3</sub>	MoO <sub>3</sub>	P3HT	Spiro-OMeTAD
Thickness (mm)	200	200	150	100	150
Band gap (eV)	3.2	1.55	3.8	2.13	3
Electron affinity (eV)	4.4	3.95	4	3	2.45
Dielectric permittivity (relative)	9	6.5	9	3	3
CB effective density of states ( $1\text{ cm}^{-3}$ )	$1 \times 10^{21}$	$3.97 \times 10^{18}$	$2.2 \times 10^{18}$	$1 \times 10^{21}$	$2.2 \times 10^{18}$
VB effective density of states ( $1\text{ cm}^{-3}$ )	$2 \times 10^{20}$	$3.97 \times 10^{18}$	$1.8 \times 10^{19}$	$1 \times 10^{21}$	$1.9 \times 10^{19}$
Electron thermal velocity ( $\text{cm s}^{-1}$ )	$1 \times 10^7$	$1 \times 10^7$	$1 \times 10^7$	$1 \times 10^7$	$1 \times 10^7$
Hole thermal velocity ( $\text{cm s}^{-1}$ )	$1 \times 10^7$	$1 \times 10^7$	$1 \times 10^7$	$1 \times 10^7$	$1 \times 10^7$
Electron mobility ( $\text{cm}^2 \text{ Vs}^{-1}$ )	20	2	3	$10^{-5}$	$2 \times 10^{-4}$
Hole mobility ( $\text{cm}^2 \text{ Vs}^{-1}$ )	10	2	6	$10^{-5}$	$2 \times 10^{-4}$
Shallow uniform donor density ND ( $1\text{ cm}^{-3}$ )	$10^{18}$	$10^{13}$	$10^{17}$	—	—
Shallow acceptor density, NA ( $1\text{ cm}^{-3}$ )	—	—	$1.8 \times 10^{19}$	$10^{16}$	$2 \times 10^{19}$

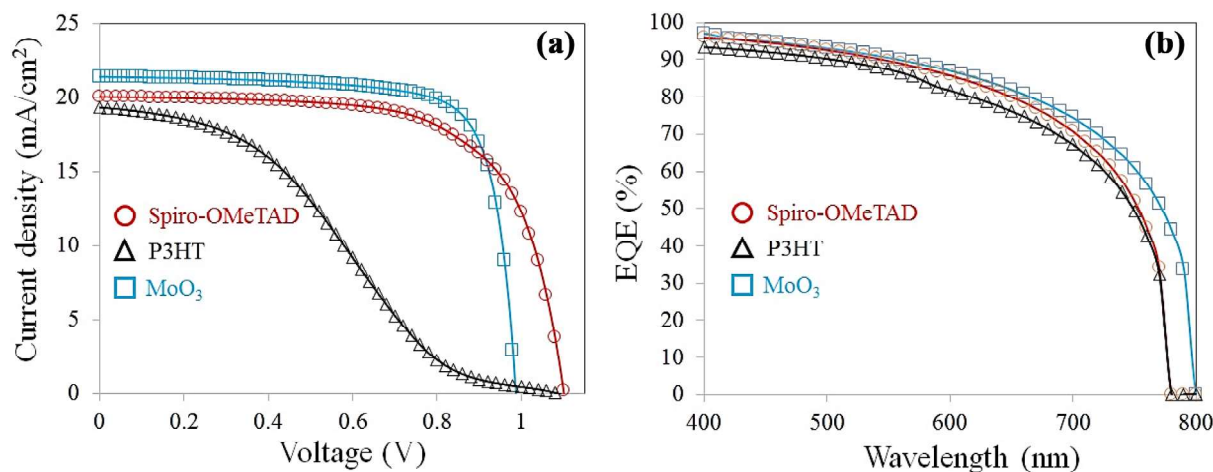


**Figure 2.** (a)  $J-V$  and (b) EQE curves of devices with different HTMs of solar cells based on  $\text{MAPbI}_3$ .

**Table 2.** Photovoltaic parameters of perovskite solar cells with different absorber layers.

HTM	$V_{OC}$ (V)	$J_{SC}$ (mA cm <sup>-2</sup> )	FF (%)	$\eta$ (%)
MoO <sub>3</sub>	0.98	21.38	76.49	16.12
Spiro-OMeTAD	1.10	20.10	66.46	14.67
P3HT	1.08	19.32	31.45	6.60

2.36  $\times$  10<sup>20</sup> and 6.32  $\times$  10<sup>20</sup> cm<sup>-3</sup> s<sup>-1</sup> happen at the  $\text{MAPbI}_3/\text{HTM}$  interface in devices with  $\text{MoO}_3$ , spiro-OMeTAD and P3HT, respectively. The solar cell efficiency with ITO/TiO<sub>2</sub>/ $\text{MAPbI}_3/\text{P3HT}/\text{Ag}$  structure is lowered due to greater electron recombination at the  $\text{MAPbI}_3/\text{P3HT}$  interface. The large distance between the valence band of  $\text{MAPbI}_3$  and HOMO of P3HT could provide a path for electron recombination which limits further improvement of device performance.

This higher recombination rate affects the short circuit current density and reduces it from 21.38 (in a device with  $\text{MoO}_3$ ) to 19.32 mA cm<sup>-2</sup> (in a device containing P3HT).

These results show that in a device with  $\text{MoO}_3$ , the  $\text{MAPbI}_3$  layer absorbs the incident photons up to 800 nm (with energies  $>1.55$  eV) to create the electron–hole pairs. These photo-generated carriers are almost separated and transported to the  $\text{MoO}_3$  and TiO<sub>2</sub> layers by the built-in field with minimum recombination.

By irradiating the light to the solar cell, excitons are created in the absorber layer. As the result, some states

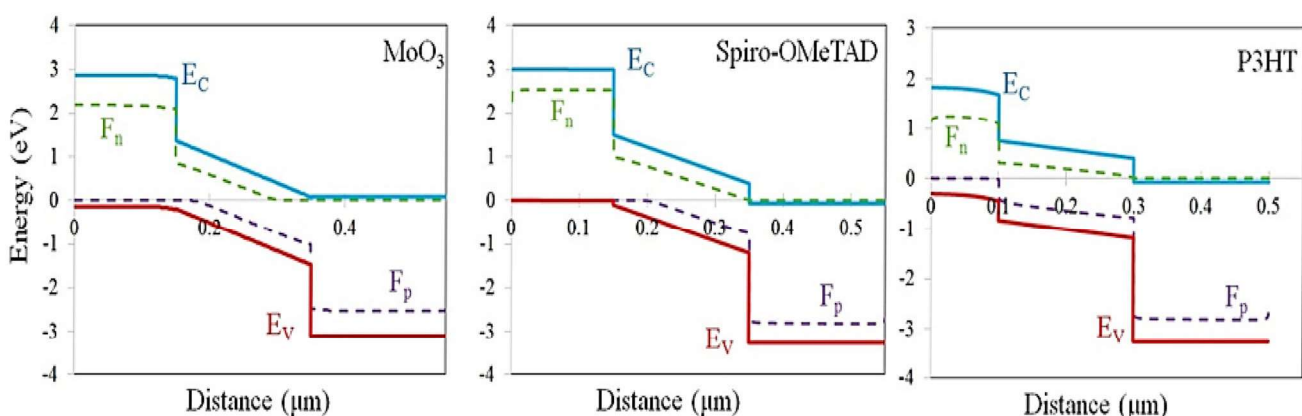


**Figure 3.** Energy levels of conduction ( $E_C$ ), valence ( $E_V$ ), Fermi level of electrons ( $F_n$ ) and holes ( $F_p$ ) in devices based on  $\text{MAPbI}_3$  perovskite with different HTMs.

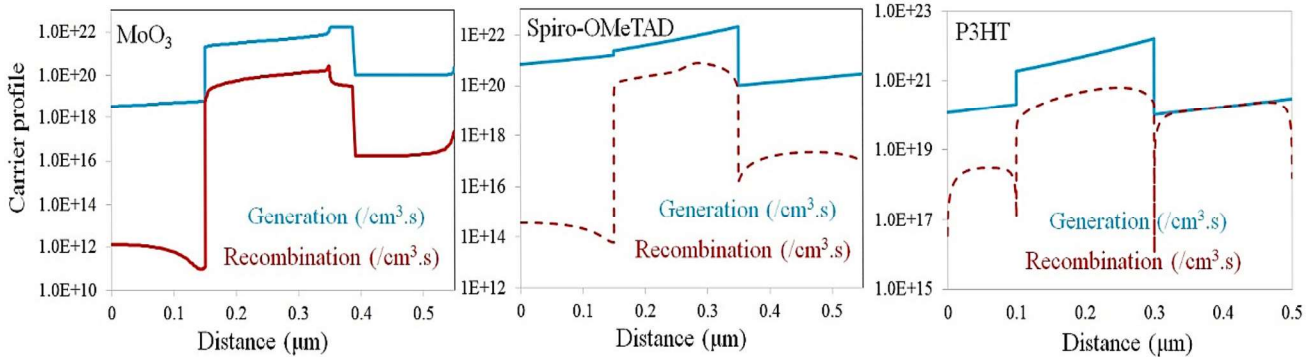


**Figure 4.** Electron–hole generation and recombination rates in devices based on MAPbI<sub>3</sub> perovskite with different HTMs.

below Fermi level ( $E_F$ ) would be empty and the corresponding number of states above this level would be filled with the excited electrons. Therefore, the equilibrium electron and hole concentrations ( $n$  and  $p$ ) are:

$$n = \int_{E_C}^{\infty} g_c(E)f(E)dE = \frac{2N_C}{\sqrt{\pi}} F_{1/2}\left(\frac{E_F - E_C}{kT}\right), \quad (5)$$

$$p = \int_{-\infty}^{E_V} g_v(E)[1-f(E)]dE = \frac{2N_V}{\sqrt{\pi}} F_{1/2}\left(\frac{E_V - E_F}{kT}\right), \quad (6)$$

where  $g_c(E)$ ,  $g_v(E)$ ,  $F_{1/2}$ ,  $k$  and  $T$  are the density of states in the conduction band and valence band, Fermi–Dirac integral of order  $\frac{1}{2}$ , Boltzmann's constant and Kelvin temperature, respectively.

While  $g_c(E)$  and  $g_v(E)$  are given by

$$g_c(E) = \frac{m_n^* \sqrt{2m_n^*(E - E_C)}}{\pi^2 \hbar^3}, \quad (7)$$

$$g_v(E) = \frac{m_p^* \sqrt{2m_p^*(E_V - E)}}{\pi^2 \hbar^3}, \quad (8)$$

where  $m_n^*$ ,  $m_p^*$ ,  $E_C$ ,  $E_V$  and  $\hbar$  are electron effective mass, hole effective mass, conduction band, valence band and reduced Planck constant, respectively. The effective densities of states in the conduction band and valence band are given by

$$N_C = 2\left(\frac{2\pi m_n^* k T}{h^2}\right)^{3/2}, \quad (9)$$

$$N_V = 2\left(\frac{2\pi m_p^* k T}{h^2}\right)^{3/2}. \quad (10)$$

The carrier concentrations in solar cells with different HTMs under illumination are shown in figure 5.

In figure 5,  $n$  and  $p$  denote electron and hole concentrations, respectively. It could be observed that the carrier concentration is almost smooth in both electron transport material (ETM, TiO<sub>2</sub>) and HTMs. Electron and hole concentrations in these layers are constant. But a significant change in carriers could be seen obviously in the absorber layer. In the interface of TiO<sub>2</sub>/MAPbI<sub>3</sub>, the majority carrier concentration ( $n$ ) begins to decrease,

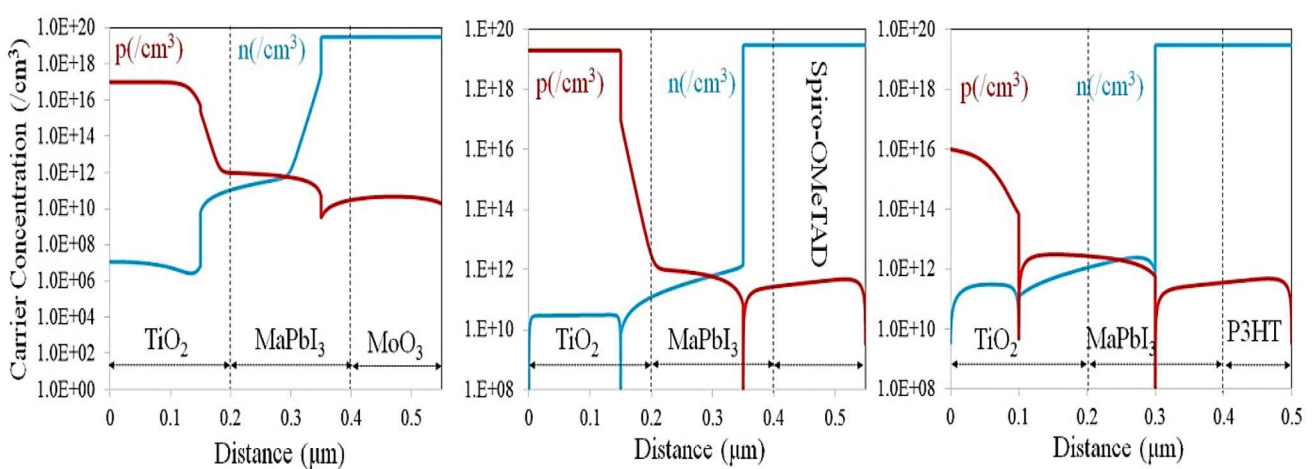


**Figure 5.** Carrier concentrations in devices based on MAPbI<sub>3</sub> perovskite with different HTMs.

while minority carrier concentration ( $p$ ) begins to increase, due to the creation of excitons under illumination. Similarly, in the  $\text{MAPbI}_3$ /HTM interface,  $n$  starts to increase, while  $p$  starts to decrease. The carrier concentration of  $n$  and  $p$  is constant across ETMs and HTMs.

### 3. Conclusion

In summary, three solar cells based on perovskite ( $\text{MAPbI}_3$ ) with different HTMs ( $\text{MoO}_3$ , spiro-OMeTAD and P3HT) with ITO/TiO<sub>2</sub>/ $\text{MAPbI}_3$ /HTM/Ag structures were investigated. Among the three HTMs, a device containing  $\text{MoO}_3$  showed the maximum PCE of 16.12% under AM 1.5G illumination of 1000 W m<sup>-2</sup> intensity. Charge extraction and electron–hole recombination processes were explained in devices. It was concluded that charge recombination at the interfaces, limits further improvement of device performance. Maximum recombination rate of  $6.32 \times 10^{20}$  cm<sup>-3</sup> s<sup>-1</sup> occurred at the  $\text{MAPbI}_3$ /P3HT interface which leads to minimum PCE of 6.6% with  $V_{\text{OC}} = 1.08$  V,  $J_{\text{SC}} = 19.32$  mA cm<sup>-2</sup> and FF = 31.45%. While maximum PCE of 16.12% with  $V_{\text{OC}} = 0.98$  V,  $J_{\text{SC}} = 21.38$  mA cm<sup>-2</sup> and FF = 76.49% was obtained for devices containing  $\text{MoO}_3$ .

### References

- [1] Mazzio K A and Luscombe C K 2014 *J. Chem. Soc.* **44** 90
- [2] Tress W, Marinova N, Inganäs O, Nazeeruddin M K, Zakeeruddin S M and Graetzel M 2014 *40th PVSC*, p. 1563
- [3] Zhong M, Yang D, Zhang J, Shi J, Wang X and Li C 2012 *J. Sol. Energy* **96** 165
- [4] Nithya K and Sudheer K 2020 *Optik* **217** 164790
- [5] Chen M, Ju M G, Carl A D, Zong Y, Grimm R L, Gu J *et al* 2018 *Joule* **2** 570
- [6] Wang G, Dong W, Gurung A, Chen K, Wu F, He Q *et al* 2019 *J. Power Sources* **432** 54
- [7] Hu M, Wu X, Tan W L, Tan B, Scully A D, Ding L *et al* 2020 *ACS Appl. Mater. Interfaces* **12** 8270
- [8] Li M, Wang Y, Xu H, Zhang H, Zhang J, Zhu Y *et al* 2020 *J. Mater. Sci.* **55** 12273
- [9] Simchi H, McCandless B E, Meng T, Boyle J H and Shafarman W N 2013 *MRS Online Proc. Library* **1538** 178
- [10] Hori T, Shibata T, Kittichungchit V, Moritou H, Sakai J and Kubo H 2009 *J. Thin Solid Films* **518** 525
- [11] Burgelman M, Nollet P and Degrave S 2000 *J. Thin Solid Films* **361** 532
- [12] Ahmed S, Jannat F, Khan M A and Alim M A 2021 *Optik* **225** 165765
- [13] Belisle R A, Jain P, Prasanna R, Leijtens T and McGehee M D 2016 *ACS Energy Lett.* **1** 560
- [14] Bilby D, Frieberg B, Kramadhati S, Green P and Kim 2014 *ACS Appl. Mater.* **6** 14974
- [15] Hori T, Moritou H, Fukuoka N, Sakamoto J, Fujii A and Ozaki M 2010 *J. Mater.* **3** 4921
- [16] Li Z, Chen J, Li H, Zhang Q, Chen Z, Zheng X *et al* 2017 *RSC Adv.* **7** 41908
- [17] Liu G, Xi X, Chen R, Chen L and Chen G 2018 *J. Renew. Sustain. Energy* **10** 043702
- [18] Li S, Cao Y L, Li W H and Bo Z S 2021 *Rare Metals* **11** 1
- [19] Minemoto T and Murata M 2015 *Sol. Energy* **133** 14
- [20] Alnuaimi A, Almansouri I and Nayfeh A 2016 *J. Comput. Electron.* **15** 1118